Experimental and numerical investigations of 3D-printed glass fiber reinforced onyx composites with infill patterns

Daouda Nikiema, Pascale Balland, Alain Sergent

Accepted Manuscript.

Cite as :

D. Nikiema, P. Balland, A. Sergent, Experimental and numerical investigations of 3D-printed glass fiber reinforced onyx composites with infill patterns, (2024). https://doi.org/10.1177/07316844241247901.

Experimental and Numerical Investigations of 3D Printed Glass Fiber Reinforced Onyx Composites with Infill Patterns

Daouda Nikiema ; Pascale Balland ; Alain Sergent

Université Savoie Mont Blanc, SYMME, F-74000 Annecy, France

Corresponding author: Daouda Nikiema

Email: daouda.nikiema@univ-smb.fr; daoudanikiema94@gmail.com

Phone / Fax: +33 4 50 09 65 67 / +33 4 50 09 65 43

Abstract

The lightweighting of 3D-printed components is achievable by using infill patterns and the ability to adjust their density. In this context, performing a mechanical characterization and numerical simulation of the printed parts is imperative. This manuscript conducts experimental and numerical investigations on 3D-printed composites (onyx/glass fibers) that considers the infill pattern, walls, roofs, and floors of the samples. A numerical homogenization approach was adopted to identify the elastic mechanical parameters of the infill patterns. The results demonstrated the homogenization tool's effectiveness in predicting the mechanical parameters of the infill patterns. Relationships correlating the infill density and each homogenized mechanical parameter were established, enabling the calculation of each mechanical parameter based on the used infill pattern and its density without reiterating the mechanical homogenization. Regarding the simulation of specimens under tension and flexure, the results indicated that the prediction error of the elastic modulus ranged between 2.87% and 11.84% for tension and between 4.42% and 8.45% for 3-point bending, respectively. The simulation of 3D-printed composites, considering all constituent elements of the specimens, allowed for examining stress fields in each element and identifying areas of highest and lowest stress. These findings can contribute to predicting the behavior of 3D-printed composites in the context of addressing engineering problems.

Keywords: 3D-Printed Composite; Infill Patterns; Mechanical Homogenization; Numerical Simulations; Tensile Test; 3-Point Bending Test

1 Introduction

Since the late 1980s, new manufacturing processes have emerged, starting with Stereolithography (SLA) as the first to enter the market. Technological advancements have led to other processes gaining prominence, including Fused Deposition Modeling (FDM), Selective Laser Sintering (SLS), Selective Laser Melting (SLM), and others. These manufacturing processes are combined with conventional methods in numerous industries, including automotive, rail, aerospace, space exploration, medical [1,2], and most recently, building construction [3]. The benefits are acknowledged, such as shorter production times and minimized costs, lessened waste and scrap, and notably, the capability to produce parts with more complex geometric shapes [4,5]. This method minimizes human resource usage, post-processing requirements, and energy consumption [6]. Another significant advantage of this method is its ability to print lightweight parts. This is made possible through infill patterns, which are typically complex structures with low density. To achieve the optimal design of these components, engaging in mechanical characterization, anticipating mechanical properties, and simulating the infill patterns numerically is critical.

There are several variations of infill patterns, the most common of which are solid, triangular, hexagonal, gyroscopic, and rectangular. These patterns may differ according to the printer model. In studies, the pattern's relative or infill density is typically the most critical parameter to consider. Bárnik et al. [7] demonstrated that specimens with a rectangular pattern have a higher maximum tensile strength than those with hexagonal and triangular patterns when the infill density is equal. In contrast, Ali et al. [8] showed in their research that 3D-printed parts (carbon fiber composite parts) with a triangular pattern are stronger than those with hexagonal and rectangular patterns at the same infill density. In [9], research findings demonstrated a significant effect of infill density on the mechanical properties of 3D-printed PLA (polylactic acid) parts. Specifically, the maximum tensile stress increases from 427 to 792 MPa for rectangular pattern specimens with densities ranging from 20% to 100%. In another study, Zhang et al. [10] found that the increased density of the honeycomb-patterned printed specimens resulted in higher flexural strength. Characterizing and predicting the mechanical parameters of infill patterns play a crucial role in 3D printing. It is, therefore, essential to ensure their accuracy and reliability.

Considering the geometric shapes of infill patterns, their mechanical behaviors are generally anisotropic. Homogenization techniques simplify the solving of engineering problems and the identification of mechanical parameters. Two principal methods are commonly employed: analytical and numerical approaches. In this context, Malek et al. [11] established the homogenized properties of hexagonal patterns using both homogenization techniques and found low relative errors. These analytical methods have limitations in scenarios where the pattern structure is highly complex, such as in the case of the gyroid. In such cases, the most appropriate solution is to use numerical homogenization methods [12]. Lei et al. [13] identified the elastic mechanical parameters of polylactic acid (PLA) specimens by identifying a Representative Volume Element (RVE) and applying periodic boundary conditions (PBCs). In [14], the mechanical properties of composite parts made of glass/epoxy and carbon/epoxy were calculated by applying mechanical homogenization with periodic boundary conditions. In the studies of Moeini et al. [15], the homogenized mechanical parameters of PLA-printed specimens were determined using two analytical models—the Gibson and Malek models—and the numerical homogenization method. The results demonstrated that analytical models and the numerical method accurately predicted the mechanical parameters with acceptable errors. Generally, research is carried out on several levels, including the meso-scale and macro-scale. At the meso-scale, homogenized mechanical parameters of the representative unit cell or pattern are determined. These parameters are then employed at the macro-scale to replicate the overall behavior of printed parts. To

date, research has not adequately explored the correlation between pattern and infill density in terms of homogenized mechanical parameters, the behavior of printed samples with patterns, and the analysis of different components of the samples.

The study analyzes the mechanical behavior of onyx/glass fiber specimens. The objective is to determine the homogenized mechanical properties of hexagonal and triangular patterns based on infill densities. The study analyzes the mechanical behavior of onyx/glass fiber specimens. The resulting parameters will be utilized for macro-scale examinations of the specimens' behavior. The numerical simulations additionally consider the specimens' walls, roofs, and floors. This research offers valuable insight for engineers in design offices, who can use the correlations between density and infill pattern to determine homogenized mechanical parameters and carry out numerical simulations on the behavior of composite specimens. The objective of this work has been to achieve this goal successfully. Section 2 describes the methods used, including specimen printing, mechanical tests, and numerical simulations. The results of our experiments and numerical simulations (including numerical homogenization and tensile and bending simulations) are presented in Section 3. Finally, the conclusions drawn from this study are outlined in Section 4.

2 Material and method

2.1 3D printing system and sample preparation

The study utilized the Markforged X7 3D printing technology. This printer features dual nozzles that facilitate the production of thermoplastic matrix parts with continuous fibers. The first nozzle prints the thermoplastic matrix layer-by-layer, while the second nozzle prints the continuous fiber reinforcement.

The printer's thermoplastic matrices are primarily composed of polyamide 6 (PA6), also known as nylon. The commercial names for these materials are onyx (a blend of PA6 and short carbon fibers), onyx FR (flame retardant), onyx FR-A (aeronautic flame retardant), nylon, and polylactic acid (PLA). Kevlar, carbon, and glass continuous fibers are primarily used as reinforcements.

The cloud-based software (Eiger), developed by Markforged, enables access to several printing parameters. The essential printing parameters for the thermoplastic matrix involve the infill pattern and density, number of roofs and floors, layer thickness, and number of walls. This printer offers five infill patterns: solid, triangular (typically recommended by the manufacturer), hexagonal, rectangular, and gyroid. This article will explore only the triangular and hexagonal patterns with varying infill densities, as shown in Figure 1. Designations have been assigned to these specimens to facilitate understanding of the documents. The specimens featuring triangular patterns at 37% and 55% infill density have been labeled as T37 and T55, respectively, while those exhibiting hexagonal patterns at 27% and 62% infill density have been labeled as H27% and H62%. A summary of the key parameters can be found in Table 1.

The key parameters for reinforcement comprise the printing mode (isotropic or concentric), number of layers, and orientation angles. In this study, the reinforcements used are concentric 3D-printed glass fibers consisting of layers oriented at an angle of 0° with respect to the longitudinal axis of the specimens.

The printed specimens have a rectangular cross-section and conform to the ASTM D638 and ASTM D3039 geometry and dimension standards (Figure 2). The specimens were designed using Inventor 2022 educational software and printed based on specific parameters. Figure 3 shows the cross-

sectional details of the specimens studied, with four layers each of walls, roofs, and floors, plus ten layers of triangular or hexagonal infill for the walls, 13 layers for the roof, and four layers of 0° fibers that were printed, bonded to the walls in the longitudinal direction.

Table 1. General printing parameters

Printing parameters	Specifications
Thermoplastic - Fibers	Onyx – Glass fibers
Pattern[1] – density (%)	Triangular – 37, 45 and 55%
Pattern[2] – density (%)	Hexagonal – 27, 40, 50 and 62%
Layer thickness – wall width (mm)	0.1 – 0.4 (fixed values)
Walls (contours) count	4
Roof and & floor layers	4
Fiber printing mode – angle (°)	Isotropic – 0°
Fiber layers count	4

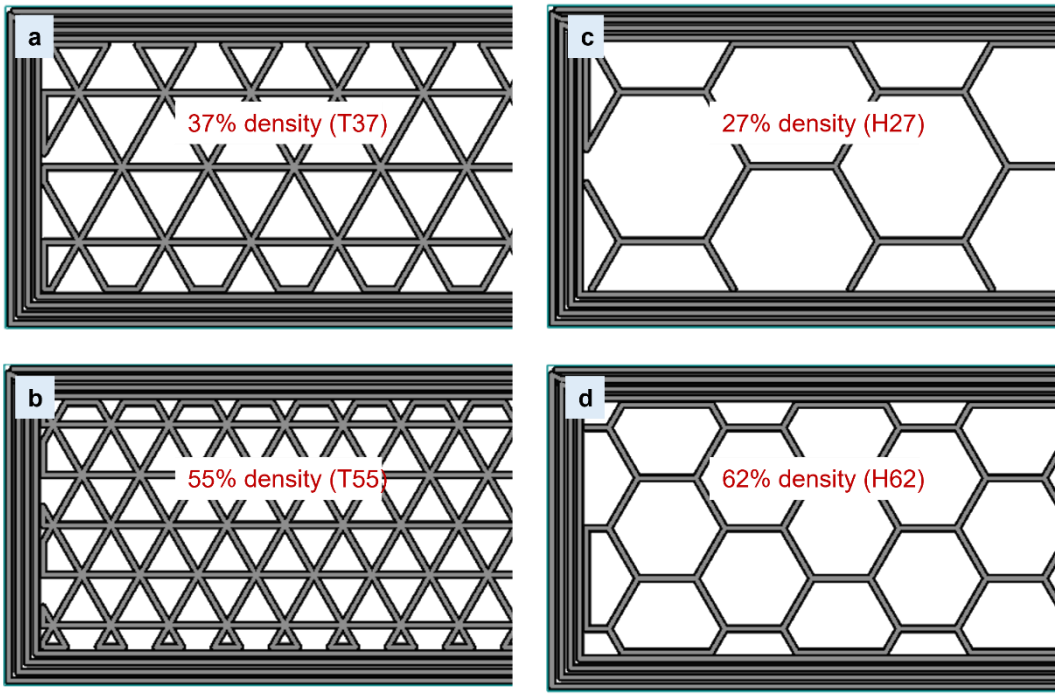

Figure 1: Views of the infill patterns and their respective densities. a – b: triangular pattern (37% and 55% density), c – d: hexagonal pattern (27% and 62% density). 37% and 27% are the default densities, and 55% and 62% are the maximum densities.

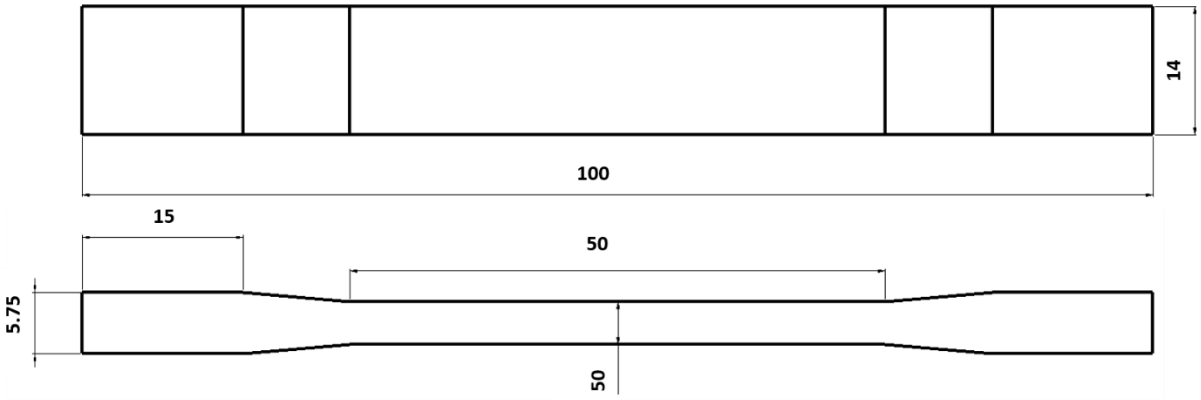

Figure 2: Sample dimensions (in millimeters).

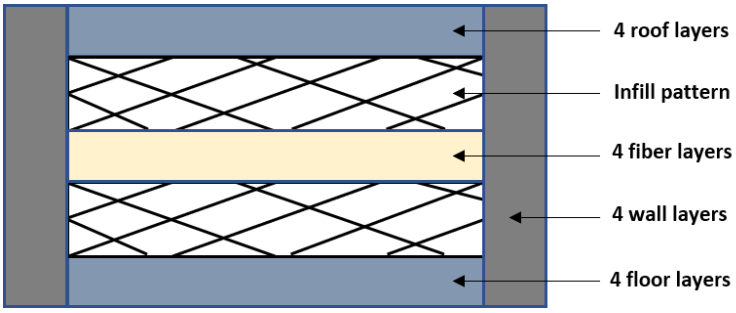

Figure 3: Simplified section of printed samples.

2.2 Experimental and testing conditions

Based on the slicer parameters, the samples were 3D printed. After printing, the specimens were subjected to tensile and bending tests using an Instron 5569 universal testing machine equipped with a 50 kN load cell, as shown in Figure 4. Tensile strain was measured with an extensometer that had a maximum strain of 40%. Bending deflection was considered as the punch displacement of the machine. Specimens were loaded until failure at a 10 mm/min test rate, and data were recorded at a data acquisition frequency of 20 Hz. Each test required a minimum of three samples, and the mean elastic modulus was taken into consideration.

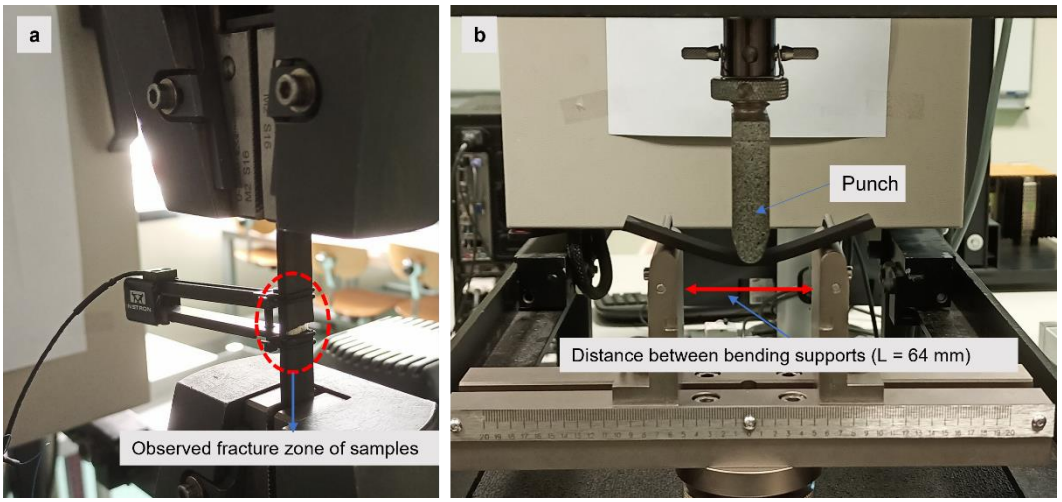

Figure 4: Experiment testing. Tensile test (a) and bending test (b).

Tensile elastic modulus was calculated using formula (1) from ASTM D3039.

$$E = \frac{\sigma_2 - \sigma_1}{\varepsilon_2 - \varepsilon_1} \quad (1)$$

Where σ_1 and σ_2 are the stress values at deformation $\varepsilon_1 = 0.1\%$ et $\varepsilon_2 = 0.3\%$, respectively. Stress was calculated using equation (2)

$$\sigma = \frac{F}{b * h} \quad (2)$$

Here, F is the tensile force, $b = 14\ mm$ and $h = 4\ mm$ are the width and the thickness of the specimen, respectively.

Bending elastic modulus was calculated according to ASTM D790 standard using equation (3) to (5)

$$\sigma_f = \frac{3 * F * L}{2 * b * h^2} \quad (3)$$

$$\varepsilon_f = \frac{6*s*h}{L^2} \quad (4)$$

$$E_f = \frac{\sigma_{f2}-\sigma_{f1}}{\varepsilon_{f2}-\varepsilon_{f1}} \quad (5)$$

The bending stresses, strain, and Young's modulus are represented by σ_f, ε_f, and E_f, respectively, where F represents the bending load. The width and thickness of the specimen are represented by b and h, respectively, and L and s represent the distance between the two bending supports and the bending deflection of the specimen recorded during the test. The bending stresses at bending deformation $\varepsilon_{f1} = 0.25\%$ and $\varepsilon_{f2} = 0.5\%$ are represented by σ_{f1} and σ_{f2}, respectively.

2.3 Numerical simulations

In this study, numerical homogenization of elastic mechanical properties for infill patterns and simulation of tensile and 3-point bending tests were performed. The aim is to forecast the mechanical characteristics and behavior of samples manufactured with triangular and hexagonal infill patterns. Figure 5 shows the numerical model for the tensile and bending test. The models display boundary conditions and mechanical loads. For the tensile model, fixed boundary conditions and a linear displacement speed are applied to replicate the physical tensile tests performed on the Instron machine. The same numerical parameterization is applied to the 3-point bending model, with a displacement speed of 10 mm/min, corresponding to the machine speed used during the physical tests. The tensile elastic modulus is calculated using the previous equations for the tensile model, based on the captured reaction forces and node displacement of the virtual extensometer. To calculate the bending elastic modulus, the reaction forces and punch displacement are used.

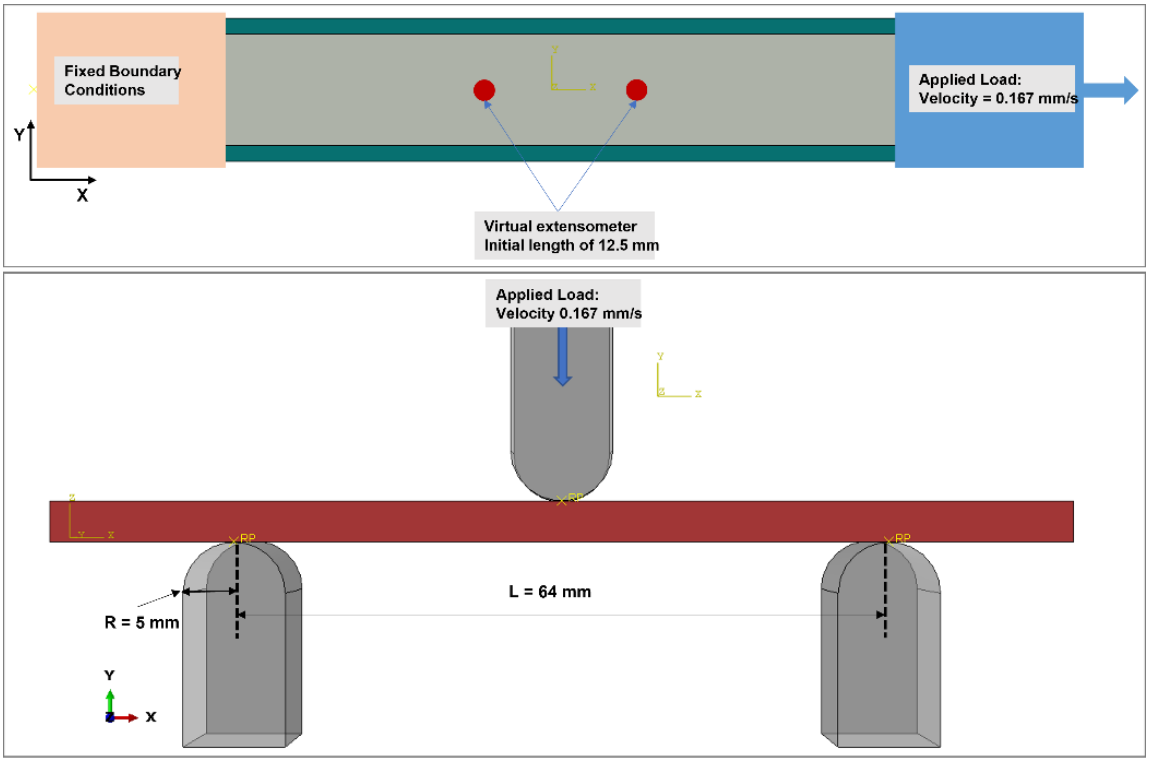

Figure 5: Numerical models: tensile test model (top) and bending test model (bottom).

Homogenization is a computational method used to determine the uniform mechanical properties of a non-uniform part, as shown in Figure 6(a). This method simplifies the microstructure of the parts to be simulated by using a homogenized structure with equivalent mechanical properties, as shown schematically in Figure 6(b). The Abaqus **Micromechanics plugin**, a homogenization tool, was used to

evaluate the mechanical properties. Using periodic boundary conditions (PBC), this tool presumes that the opposite faces of the Representative Volume Element (RVE) possess identical displacements. References [15–17] provide the mathematical formulations and procedures for homogenization implementation. To apply PCBs to a Representative Volume Element (RVE) using the Abaqus tool, the user must first select and save pairs of opposing faces in the Abaqus assembly module. The PCBs will be automatically applied to these faces when the user runs the simulation. Next, the user must select the type of mechanical loading to apply. In Abaqus, two loading modes are applicable to RVEs: deformation and stress loading (using unit loads). For this work, deformation loading was used. Elastic mechanical parameters are automatically calculated for each loading case (pure tension and pure shear), but details of the calculations are not provided by the software editor.

For each homogenization problem, identification of the RVE is mandated. RVEs were identified for the hexagonal and triangular infill patterns in this study, as depicted in Figure 6(a) and Figure 6(b), respectively. Dimensions of each pattern studied based on its density are summarizes in Table 2.

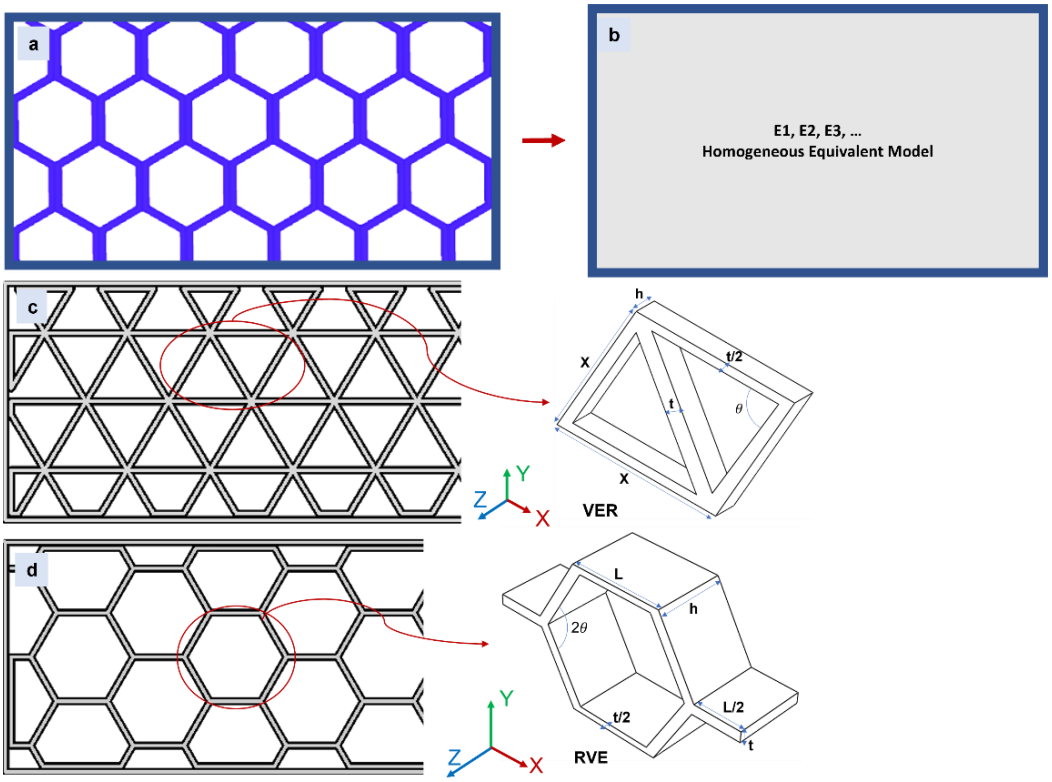

Figure 6: Homogenization principle. a) initial part; b) equivalent homogeneous part; c) triangular RVE and d) hexagonal RVE

Table 2. Dimensions of the RVE(s) studied.

Dimensions	T37	T45	T55	H27	H40	H50	H62
X (mm)	3.692	3.290	2.493				
t (mm)	0.4	0.4	0.4	0.4	0.4	0.4	0.4
h (mm)				4			
L(mm)				4.220	3.540	3.240	2.956
***θ* (°)**				60			

Once the homogenized mechanical parameters had been obtained, a numerical simulation was carried out to validate the identified parameters and predict the specimens' mechanical behavior under tensile and bending loads. The simulation considered various parts of the specimen, including the walls, roof,

floor, the homogenized infill pattern, and the glass fibers, as shown in Figure 7. The mechanical parameters utilized for simulation, excluding the infill patterns, are detailed in Table 3. In a previous article [18], the elastic modulus of the walls and solid infill (floor & roof) was determined. The elastic modulus of the glass fibers was obtained through a tensile test on a sample printed entirely with glass fibers at a 0° angle. The distribution of glass fibers in the test specimens was achieved based on the settings in the slicing software (Eiger). The fibers were printed along the length of the specimens and the dimensions of each fiber are given in Table 3.

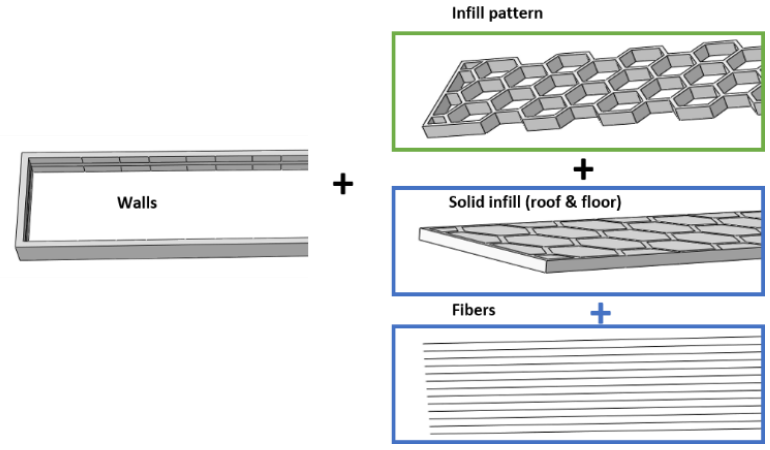

Figure 7: Different parts of the sample considered in the simulation.

Table 3. Elastic parameters used in the simulation and fiber dimensions.

	Glass fibers	Onyx (Floor-Roof)	Onyx (Walls)
Elastic modulus (MPa)	70000	1660	5400
Poisson's ratio	0.25	0.35	0.35
Glass fiber shape and dimensions			
Cross-section shape	**Length**	**Width**	**Thickness**
Rectangular	96 mm	0.57 mm	0.052 mm

3 Results and discussion

3.1 Tensile test results

The results of the tensile tests, as shown in Table 4, indicate that specimens with triangular infill patterns have a higher modulus of elasticity than those with hexagonal infill patterns. This supports the manufacturer's recommendation of the triangular pattern by default. Moreover, the mechanical strength of the triangular pattern surpasses that of the hexagonal pattern, as observed in line with the findings of Ali et al. [19]. Comparing the elastic modulus shows that the maximum density for both pattern types results in more rigid specimens than the default filling density, which is unsurprising. Bárnik et al. [7] found that specimens with different patterns do not have the same elastic modulus, even at equal density. This difference can be attributed to the volume of material consumed when printing these specimens. Other variables were also compared, such as the ratio of modulus to specimen mass and material cost. It was found that sample H62 had the best modulus to mass ratio and therefore the best performance. In terms of material cost, the observed price difference was a maximum of $ 0.17, which can be considered low. Therefore, the criterion of material cost can be left out of consideration in this study.

Table 4. Elastic modulus and material cost of tested samples (H27 and H62 are hexagonal patterned samples with 27% and 62% density, and T37 and T55 are triangular patterned samples with 37% and 55% density).

	H27	H62	T37	T55
Elastic modulus E (MPa)	2940±1	3040±104	3362±96	3510±87
Ratio E/weight (MPa/g)	625.53	645.43	637.95	630.16
Material cost (USD)	1.55	1.55	1.66	1.72

3.2 Numerical homogenization of material parameters

3.2.1 Validation of the micromechanics tool

Abaqus generated the micromechanical homogenization tool used in this article, which was initially created to compute homogenized mechanical parameters of composite materials. To evaluate the efficiency of the homogenization tool in predicting the mechanical parameters of infill patterns, an investigation of the homogenized properties of a structure with a hexagonal infill pattern was carried out. The structure consisted of aluminum material possessing an elastic modulus of E = 70 GPa and Poisson's ratio of 0.3. The size and configuration of the Representative Volume Element (RVE) for this hexagonal pattern are presented in Figure 8. The RVE was meshed with 205,128 3D finite elements of type C3D20 (20-node brick element, full integration).

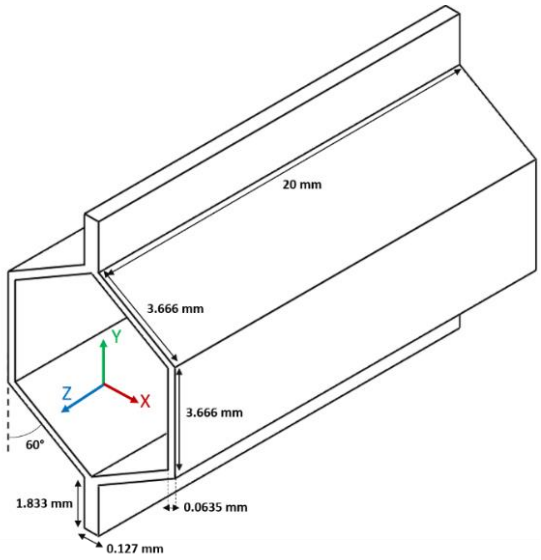

Figure 8: Tested hexagonal RVE and its dimensions.

The homogenized elastic parameters are reported in Table 5, and the density of the homogenized material is expressed in $T.mm^{-3}$ to follow the unit convention used by the Abaqus software. The results are then compared to those obtained by Catapano et al. [20], with relative errors ranging from 0.76% to 9.21%. These findings demonstrate the predictive ability of the "Abaqus Micromechanic Tool" for determining the elastic mechanical properties of infill patterns. This tool was used to determine the standardized properties of onyx-printed triangular and hexagonal patterns in the following stages of the work.

Table 5. Effective material properties for the hexagonal RVE studied

Elastic properties	Present work	Catapano et al. [20]	Error (%)
E_1 (MPa)	0.943	0.884	6.67
E_2 (MPa)	0.908	0.918	1.08
E_3 (MPa)	1830	1812	0.99
G_{12} (MPa)	0.581	0.640	9.21
G_{23} (MPa)	265	263	0.76
G_{13} (MPa)	388	391	0.76
Nu_{12}	1	0.980	2.04
Nu_{23}	0.163×10^{-3}	0.161×10^{-3}	1.24
Nu_{13}	0.170×10^{-3}	0.167×10^{-3}	1.79
Density (T.mm^{-3})	7.059×10^{-11}	6.990×10^{-11}	0.98

3.2.2 Equivalent properties of the 3D-printed pattern

After verifying the homogenization tool's capability, this section will determine the homogenized mechanical properties of triangular and hexagonal patterns. The corresponding results, dependent upon the infill pattern density, are displayed in Table 6 and Table 7.

Table 6. Elastic homogenized parameters for a triangular pattern with infill density relationships.

Elastic Parameters	T37	T45	T55	Relationships between infill density and mechanical parameters
E_{11} (MPa)	526	662	813	$-278.75 + 25.65d - 0.105d^2$
E_{12} (MPa)	526	662	813	$-278.75 + 25.65d - 0.105d^2$
E_{33} (MPa)	1226	1458	1727	$-41.25 + 38.56d - 0.116d^2$
G_{12} (MPa)	202	255	311	$-138 + 1.29d - 0.056d^2$
G_{23} (MPa)	262	327	394	$-170 + 14.61d - 0.079d^2$
G_{13} (MPa)	262	327	394	$-170 + 14.61d - 0.079d^2$
Nu_{12}	0.30	0.30	0.30	0.3 (Constant value)
Nu_{23}	0.15	0.15	0.16	$0.24 - 45x10^{-4}d + 555x10^{-7}d^2$
Nu_{13}	0.15	0.15	0.16	$0.24 - 45x10^{-4}d + 555x10^{-7}d^2$
Density x 10^{-10} (T.mm^{-3})	2.72	3.42	3.84	$-472x10^{-2} - 295x10^{-3}d - 253x10^{-5}d^2$

Table 7. Elastic homogenized parameters for a hexagonal pattern with infill density relationships.

Elastic parameters	H27	H40	H50	H62	Relationships between infill density and mechanical parameters
E_{11} (MPa)	18	31	42	59	$1.94 + 0.35d + 0.009d^2$
E_{12} (MPa)	17	31	42	58	$1,94 + 0.35d + 0.009d^2$
E_{33} (MPa)	638	718	862	940	$412.82 + 7.64d + 0.016d^2$
G_{12} (MPa)	4.15	8.06	10.98	14	$-5.28 + 0.37d - 0.001d^2$
G_{23} (MPa)	123	154	172	191	$-5.28 + 0.37d - 0.001d^2$
G_{13} (MPa)	123	154	172	191	$42.55 + 3.47d - 0.017d^2$
Nu_{12}	0.97	0.92	0.91	0.91	$0,023 - 614x10^{-6}d + 953.10^{-8}d^2$
Nu_{23}	0.014	0.013	0.017	0.022	$1.16 - 935x10^{-5}d + 863x10^{-7}d^{-2}$
Nu_{13}	0.014	0.013	0.017	0.022	$1.16 - 935x10^{-5}d + 863x10^{-7}d^{-2}$
Density x 10^{-10} (T.mm^{-3})	1.42	1.73	1.92	2.09	$543x10^{-3} + 382x10^{-4}d - 215x10^{-6}d^2$

For each parameter, a relationship with the infill pattern density is established. Figure 9 displays the elastic parameters of triangular pattern and relationships between the infill density. The deformations

resulting from the utilized loading conditions in homogenization are presented in Figure 10 and Figure 11 for the triangular and hexagonal patterns, respectively. The corresponding equation for each parameter calculated as a function of the infill pattern density is provided, most of which were determined through second-order polynomial regression. The provided equations enable the precise prediction of all the parameters required for the numerical simulation of printed parts featuring triangular or hexagonal patterns. As noted by Julien Yvonnet [21], a third-order polynomial can be implemented to interpolate the elastic parameters of 3D-printed lattice structures. However, a second-order polynomial was deemed sufficiently accurate in the present study. Certain infill pattern forms, such as lattice structures or gyroid patterns, may render analytical methods ineffective or impractical for calculating mechanical parameters, as suggested by analytical methods proposed by Gibson et al. [22]. In such cases, numerical homogenization can be considered an effective tool to determine the elastic parameters of infill patterns. The elastic parameters determined in this study are sufficient for solving common engineering problems. For more intricate issues necessitating the application of plastic mechanical parameters, the numerical homogenization tool may not suffice, leading to the need for other tools to determine plastic parameters. However, the elastic parameters calculated in this study are adequate for the numerical simulation of 3D-printed components. The homogenized material densities calculated during the homogenization process are useful for simulations that require mass, such as explicit simulations or vibration simulations. For the current simulations, which were carried out with Abaqus Standard, the homogenized densities of the model were not utilized.

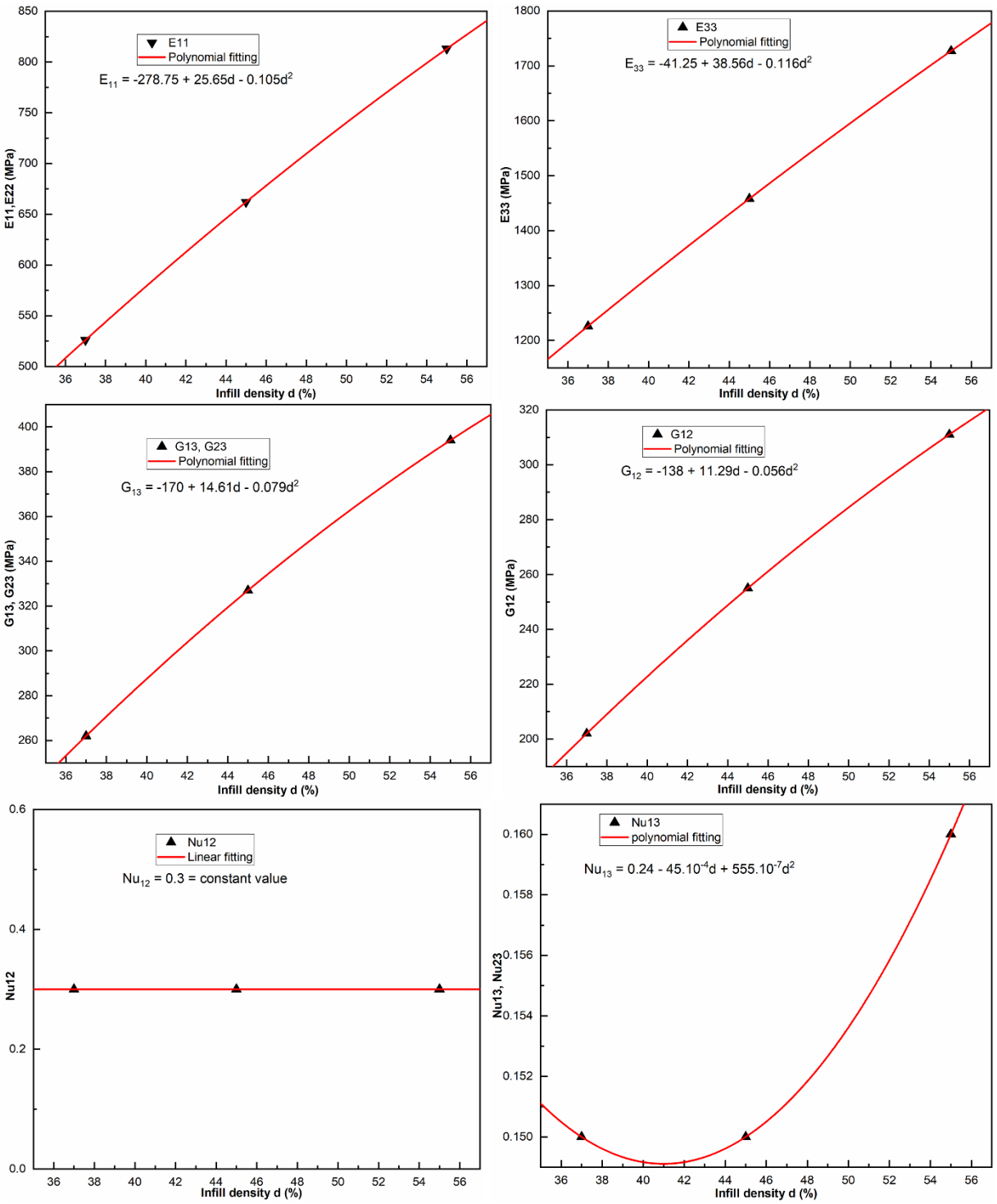

Figure 9: Relationship between homogenized mechanical parameters and infill density: the case of the triangular pattern.

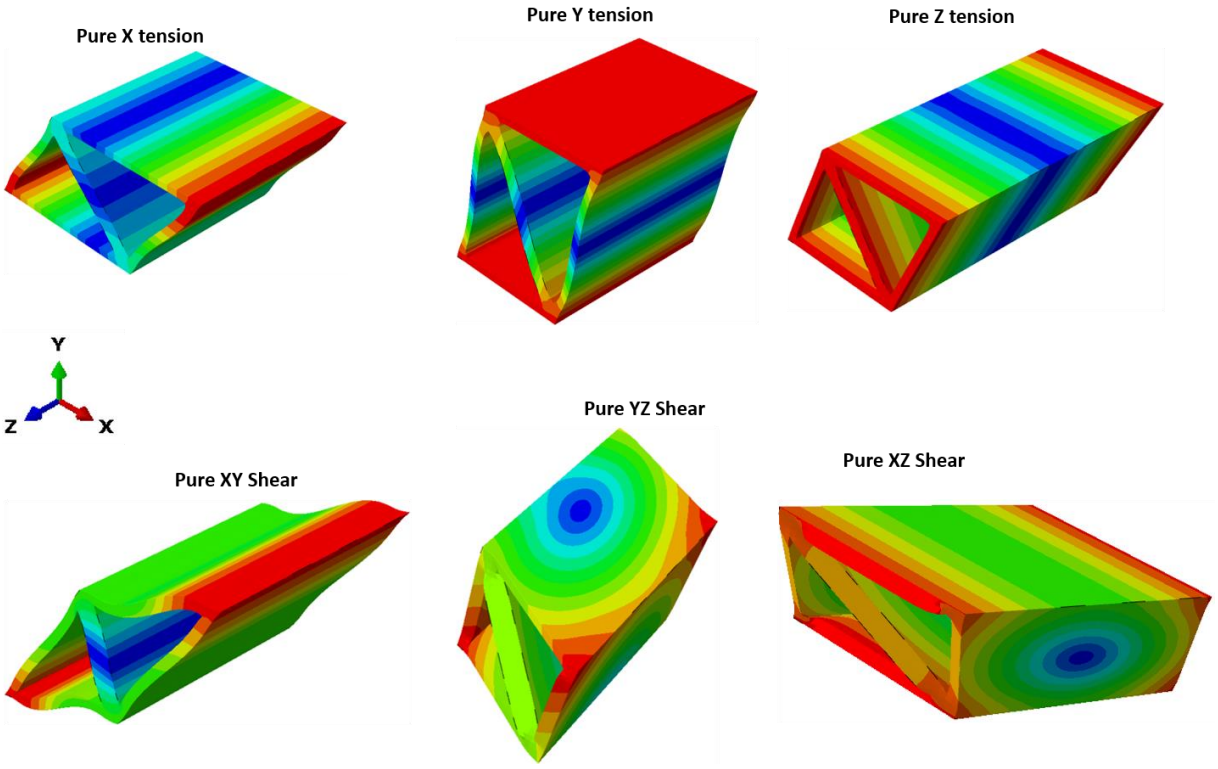

Figure 10: RVE deformations under the six homogenization load cases for the triangular pattern (x, y, z pure tension and xy, yz, xz pure shear).

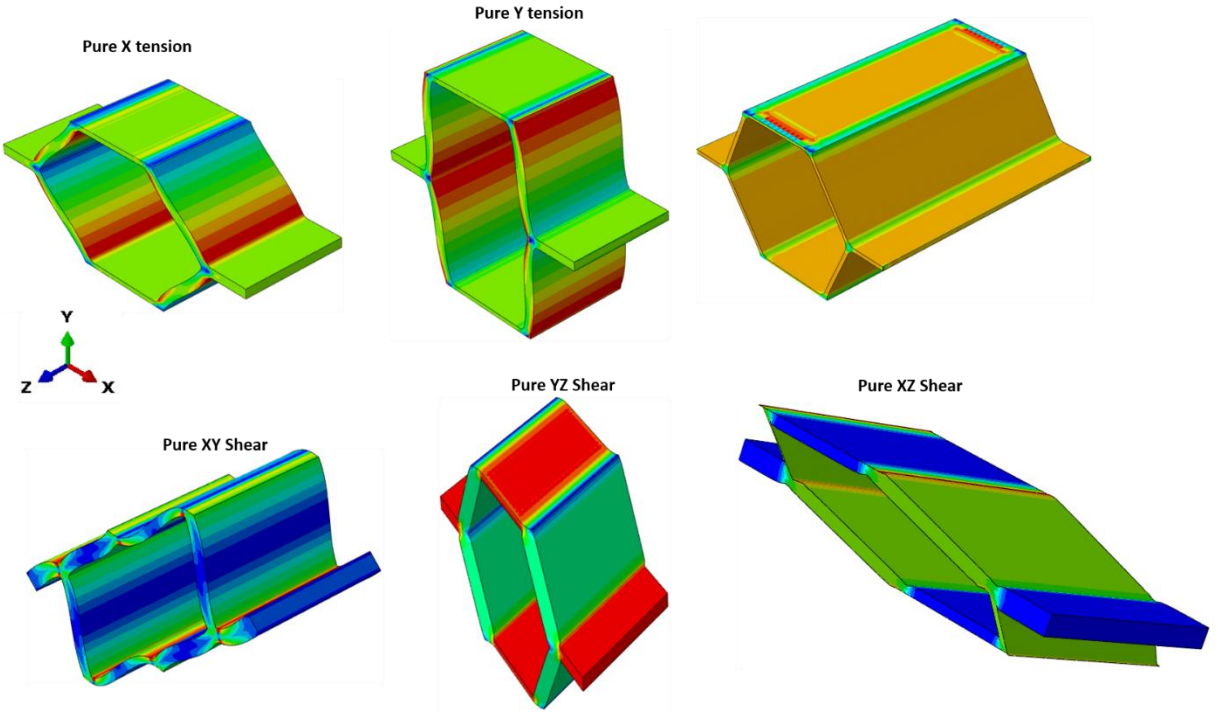

Figure 11: RVE deformations under the six homogenization load cases for the hexagonal pattern (x, y, z pure tension and xy, yz, xz pure shear).

3.3 Numerical simulations of tension and 3-point bending

The previously determined elastic parameters were used to model the mechanical behavior in the tension and three-point bending of triangular and hexagonal specimens, with infill density of 55% and 62%, respectively (The maximum infill density of the two patterns under study). Fibers were included in the simulation using the embedded element technique, where the fibers are considered type B31 (2-node 1D beam elements). Beam elements were chosen over truss elements because they do not support bending loads. Truss elements may be used to represent fibers in the numerical model if the study is limited to tensile loading. Further details on the embedded element technique can be found in [23,24]. The type C3D20 3D finite elements were utilized to model the other constituent parts of the specimen (homogenized pattern, roof, and floor). The elements are assumed to be continuously meshed with fixed connections, such as between walls and other elements, the roof and the homogenized pattern, and the floor and the pattern. Therefore, this modeling requires no friction between the components.

As shown in Table 8, the elastic modulus is the main result of the numerical simulations analyzed. Figure 12 and Figure 13 show the graphical representation of the numerical and experimental tensile and three-point bending curves (experimental curves were drawn until failure point), respectively. In Figure 14, the deformation of the numerical models for tensile and bending are shown. The stress fields in each element of the T55 specimen during three-point bending and tensile test are illustrated in Figure 15 and Figure 16, respectively while details on different parts are provided for clarity. The most stressed elements of the specimen are the glass fibers and walls, whereas the pattern experiences the least stress.

Table 8. Elastic modulus of samples in tensile and bending tests (comparison between numerical and experimental results).

	T55 (tension)	**H62 (tension)**	**T55 (bending)**	**H62 (bending)**
Experiment (MPa)	3510	3040	2216	1914
Simulation (MPa)	3611	3400	2314	2074
Error (%)	2.87	11.84	4.42	8.35

When compared to the experimental elastic moduli, the low prediction errors of the numerical elastic moduli range only from 2.87% to 11.84% for both tension and bending. This strongly indicates that the numerical models studied can predict the mechanical properties of 3D-printed parts. A previous study conducted by Tessarin et al. [25] reported an 11.63% prediction error for the tensile elastic modulus of the onyx/glass fiber composite specimen. This indicates that the prediction errors observed in the present study are still within acceptable levels compared to those reported in the literature. Nevertheless, it is challenging to predict the overall behavior of the parts. One possible explanation could be the omitted consideration of plasticity when homogenizing mechanical parameters for the patterns. In the simulation models, plasticity in the walls, roof, and floor is taken into account, while the pattern only includes elastic parameters. For the bending scenario, using C3D20 3D finite elements exhibits constraints on materials having a Poisson's ratio greater than 0.5. Incorporating these elements causes the material to stiffen beyond the plastic domain, resulting in an overestimation of stiffness in the plastic domain of the parts, as shown in Figure 13.

Homogenized numerical models offer a significant advantage in reducing simulation time. Viet et al. [26] found that a model using homogenized properties requires only 13.8 seconds of CPU time compared to the 425.7 seconds needed for the non-homogenized model. This enhancement in

simulation time renders the homogenized numerical simulation technique efficient and reliable for typical engineering problems.

The novelty of this work lies in the utilization of commercial software plugins (Abaqus) to compute homogenized mechanical properties of patterns and establish correlations that link these properties to fill density. These correlations enable users to calculate homogenized mechanical properties without having to repeat the homogenization process using the plugin or any other software. This work predicts the mechanical behavior of printed parts using the embedded element technique. It takes into account the mechanical behavior of each part compartment, including walls, patterns, filling, and fibers.

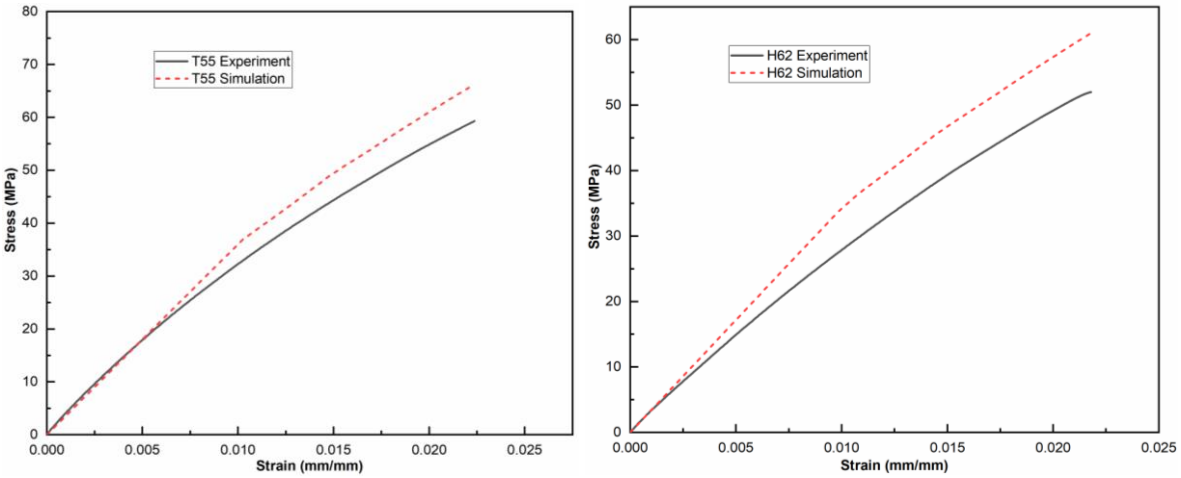

Figure 12: Comparison between experimental and numerical tensile curves (left: sample with triangular patterns and right: sample with hexagonal patterns).

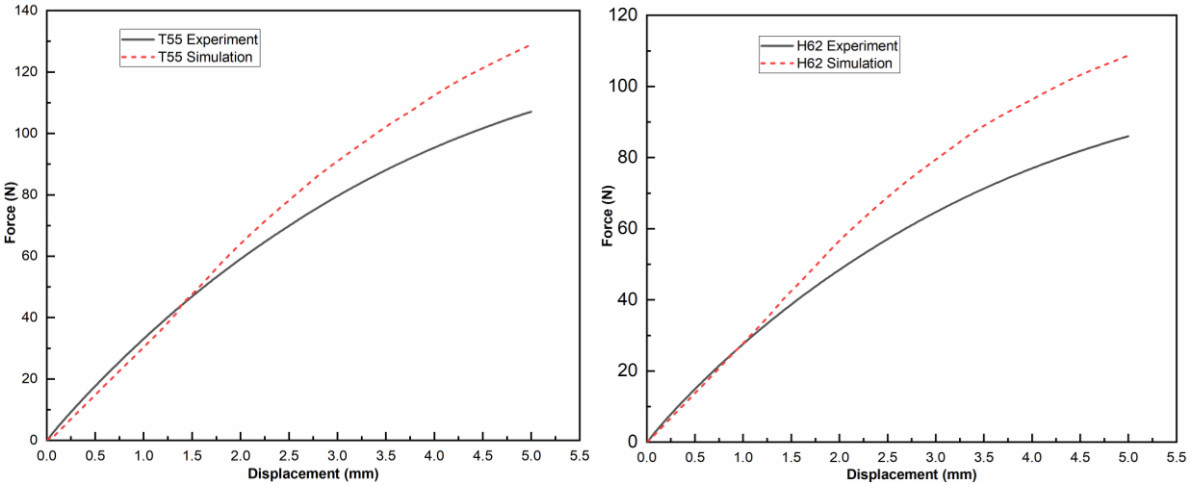

Figure 13: Comparison between experimental and numerical 3-point bending curves (left: sample with triangular patterns and right: sample with hexagonal patterns).

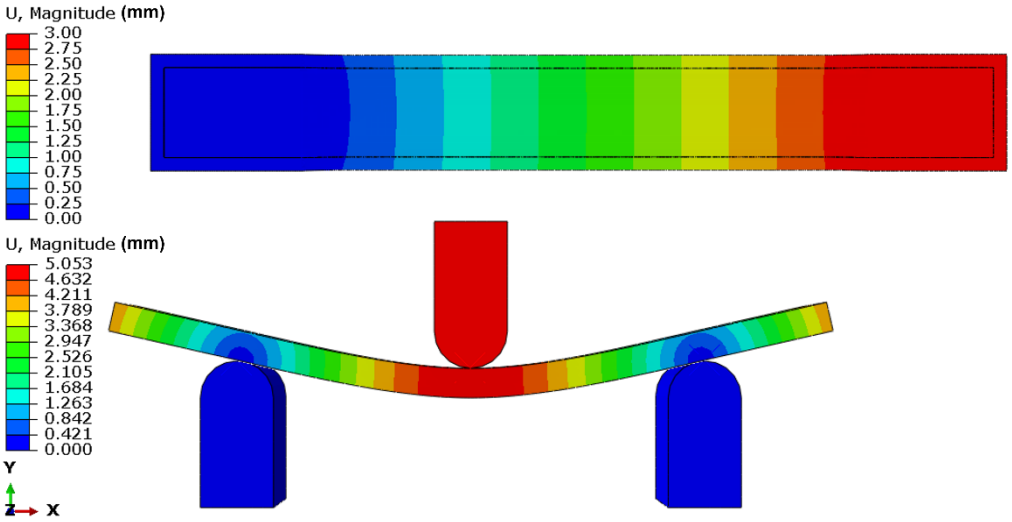

Figure 14: Deformations of the numerical models. Tensile model (top) and bending model (bottom).

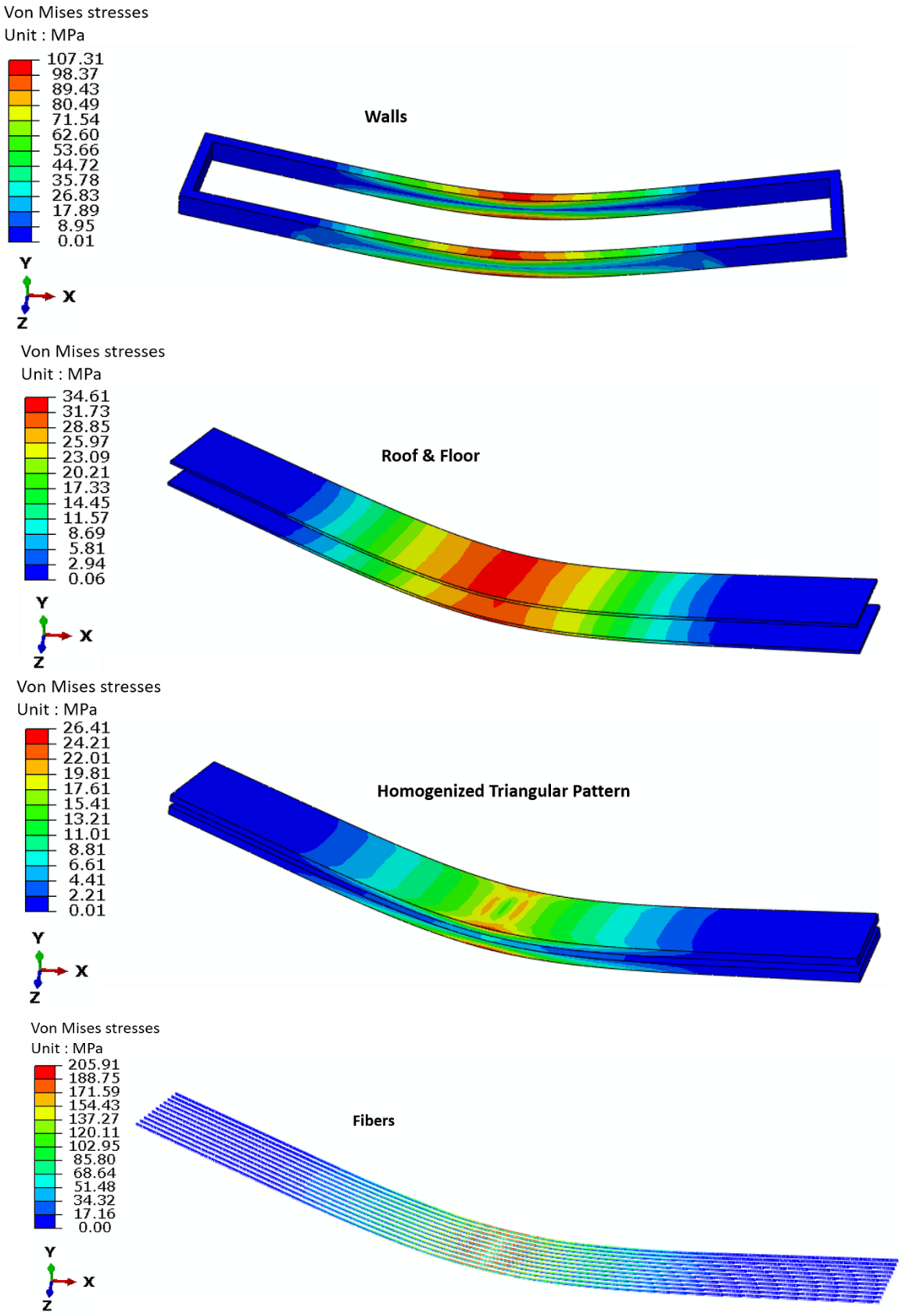

Figure 15: Details of the stress fields observed on the different parts of the T55 sample for bending test.

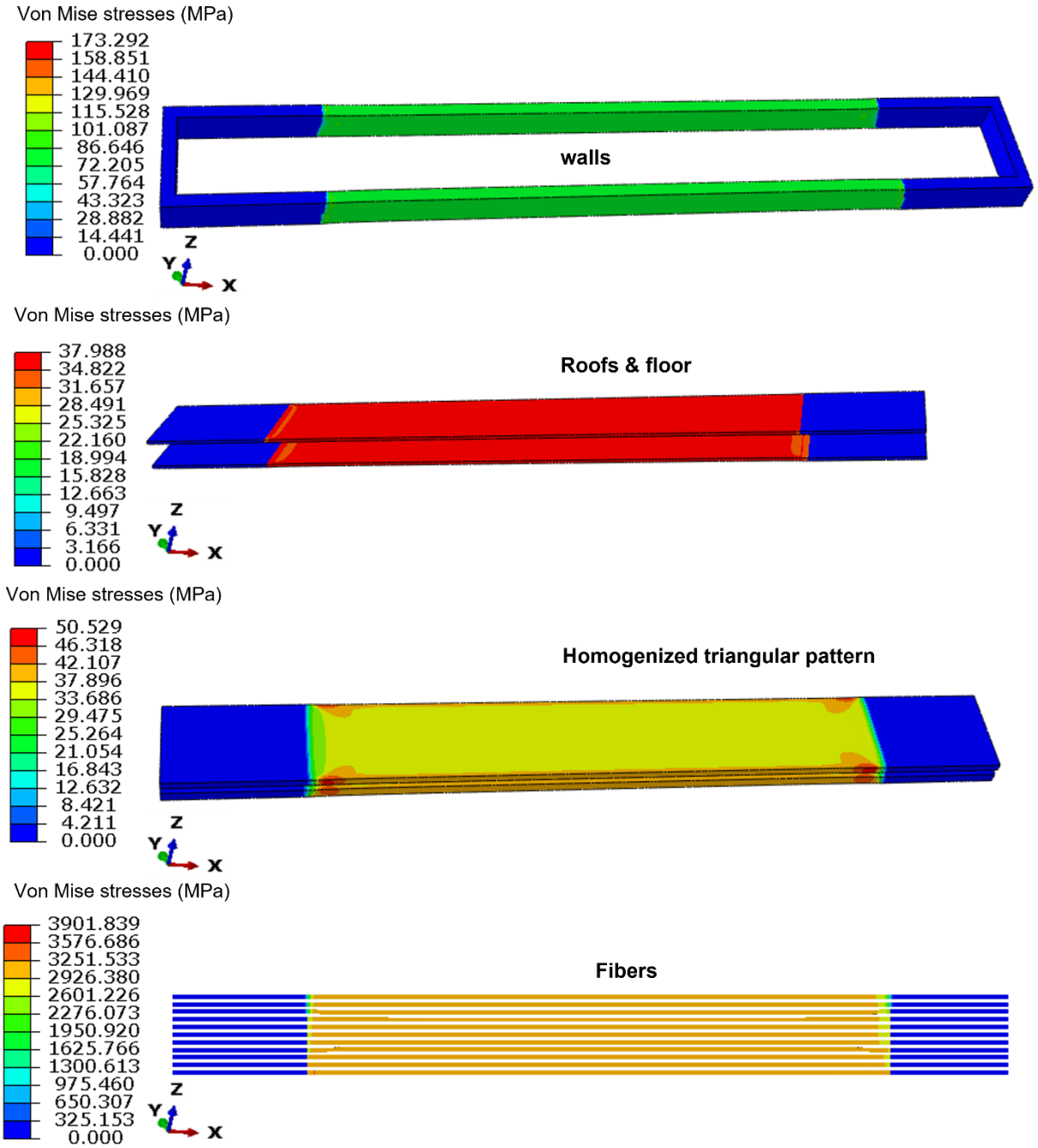

Figure 16: Details of the stress fields observed on the different parts of the T55 sample for tensile test.

4 Conclusion

Mechanical characterization, both experimental and numerical, was carried out on onyx/glass fiber composites in this study. These composites were 3D printed with hexagonal and triangular patterns. The elastic mechanical parameters of the patterns were determined using a numerical homogenization tool. The findings from the different investigations can be summarized as follows:

1/The tensile tests showed that the elastic modulus of specimens with triangular patterns was higher than that of those with hexagonal patterns. The results suggest that the triangular pattern exhibits greater stiffness than the hexagonal pattern, consistent with previous findings in the literature.

2/ Numerical homogenization was used to determine the elastic-mechanical parameters for both patterns at different filling densities. A second-order polynomial function was identified to calculate each parameter without re-homogenization. These mathematical functions allow for calculating the elastic mechanical properties of triangular or hexagonal patterns when the fill density is known.

3/ After identifying the mechanical parameters of the patterns, numerical simulations were carried out under both tensile and flexural loading conditions for the walls, roofs, and floors. Compared to experimental tests, the simulations revealed prediction errors of 2.87% to 11.84% and 4.42% to 8.45% for tensile and flexural loading, respectively.

In summary, this study identified the homogenized properties of patterns based on their fill densities, which offers significant insights for numerical simulations of specimens under mechanical stresses. The thorough examination of supplementary sections of the specimen is imperative to comprehend its stress states. This research will allow engineers to accurately predict the mechanical properties and behavior of 3D-printed composite components containing long fibers and patterns.

Declaration of Competing Interest

The authors declare that they have no known competing financial interests or personal relationships that could have influenced the work reported in this paper.

Credit authorship contribution statement

Daouda Nikiema: Conceptualization, writing, review, and editing; **Pascale Balland**: Resources, Funding acquisition, writing, review, and editing; **Alain Sergent**: Writing, review, and editing;

Data availability

Data will be made available on request.

Acknowledgment

Daouda NIKIEMA reports writing assistance was provided by the University Savoie Mont Blanc Laboratory of Systems and Materials for Mechatronics.

References

[1] R.C. Advincula, J.R.C. Dizon, Q. Chen, I. Niu, J. Chung, L. Kilpatrick, R. Newman, Additive manufacturing for COVID-19: Devices, materials, prospects, and challenges, MRS Commun. 10 (2020) 413–427. https://doi.org/10.1557/mrc.2020.57.

[2] B. Pavan Kalyan, L. Kumar, 3D Printing: Applications in Tissue Engineering, Medical Devices, and Drug Delivery, AAPS PharmSciTech. 23 (2022). https://doi.org/10.1208/s12249-022-02242-8.

[3] Sculpteo, The state of 3D PRINTING: The data you need to understand the 3D Printing world and build your 3D Printing strategy, Print. Polym. Fundam. Appl. (2015) 293–306.

[4] S.A.M. Tofail, E.P. Koumoulos, A. Bandyopadhyay, S. Bose, L. O'Donoghue, C. Charitidis, Additive manufacturing: scientific and technological challenges, market uptake and opportunities, Mater. Today. 21 (2018) 22–37. https://doi.org/10.1016/j.mattod.2017.07.001.

[5] R. Surya Teja, M. Lokesh, S. Deepak Kumar, P.S.V. Ramana Rao, 3D Printing of complex structures: Case study of Eiffel Tower, Mater. Today Proc. (2022). https://doi.org/10.1016/j.matpr.2022.12.037.

[6] A. Jandyal, I. Chaturvedi, I. Wazir, A. Raina, M.I. Ul Haq, 3D printing – A review of processes, materials and applications in industry 4.0, Sustain. Oper. Comput. 3 (2022) 33–42. https://doi.org/10.1016/j.susoc.2021.09.004.

[7] F. Bárnik, M. Vaško, M. Handrik, F. Dorčiak, J. Majko, Comparing mechanical properties of composites structures on Onyx base with different density and shape of fill, Transp. Res. Procedia. 40 (2019) 616–622. https://doi.org/10.1016/j.trpro.2019.07.088.

[8] J. John, D. Devjani, S. Ali, S. Abdallah, S. Pervaiz, Optimization of 3D printed polylactic acid structures with different infill patterns using Taguchi-grey relational analysis, Adv. Ind. Eng. Polym. Res. 6 (2023) 62–78. https://doi.org/10.1016/j.aiepr.2022.06.002.

[9] M.A. Mazlan, M.A. Anas, N.A. Nor Izmin, A.H. Abdullah, Effects of Infill Density, Wall Perimeter and Layer Height in Fabricating 3D Printing Products, Materials (Basel). 16 (2023). https://doi.org/10.3390/ma16020695.

[10] X. Zhang, C. Xu, W. Li, Z. Su, Study on the bending and shear properties of quasi-honeycomb sandwich structures considering the variable-density core design, Compos. Struct. 324 (2023). https://doi.org/10.1016/j.compstruct.2023.117517.

[11] S. Malek, L. Gibson, Effective elastic properties of periodic hexagonal honeycombs, Mech. Mater. 91 (2015) 226–240. https://doi.org/10.1016/j.mechmat.2015.07.008.

[12] P. Bean, R.A. Lopez-Anido, S. Vel, Numerical Modeling and Experimental Investigation of Effective Elastic Properties of the 3D Printed Gyroid Infill, Appl. Sci. 12 (2022). https://doi.org/10.3390/app12042180.

[13] M. Lei, Y. Wang, Q. Wei, M. Li, J. Zhang, Y. Wang, Micromechanical modeling and numerical homogenization calculation of effective stiffness of 3D printing PLA/CF composites, J. Manuf. Process. 102 (2023) 37–49. https://doi.org/10.1016/j.jmapro.2023.07.027.

[14] P. Ghabezi, N.M. Harrison, Multi-scale modelling and life prediction of aged composite materials in salt water, J. Reinf. Plast. Compos. (2023). https://doi.org/10.1177/07316844231160189.

[15] M. Moeini, M. Begon, M. Lévesque, Numerical homogenization of a linearly elastic honeycomb lattice structure and comparison with analytical and experimental results, Mech. Mater. 167

(2022). https://doi.org/10.1016/j.mechmat.2022.104210.

[16] W. Tian, L. Qi, X. Chao, J. Liang, M. Fu, Periodic boundary condition and its numerical implementation algorithm for the evaluation of effective mechanical properties of the composites with complicated micro-structures, Compos. Part B Eng. 162 (2019) 1–10. https://doi.org/10.1016/j.compositesb.2018.10.053.

[17] D.J. Wu, Z. Mei, Y. Zhu, H. Hu, Development of an ABAQUS™ plug-in for predicting composite plates stiffness with in-plane periodicity, SoftwareX. 21 (2023). https://doi.org/10.1016/j.softx.2022.101281.

[18] D. Nikiema, N.A. Sène, P. Balland, A. Sergent, Study of walls' influence on the mechanical properties of 3D printed onyx parts: Experimental, analytical and numerical investigations, Heliyon. 9 (2023) e19187. https://doi.org/10.1016/j.heliyon.2023.e19187.

[19] Z. Ali, Y. Yan, H. Mei, L. Cheng, L. Zhang, Effect of infill density, build direction and heat treatment on the tensile mechanical properties of 3D-printed carbon-fiber nylon composites, Compos. Struct. 304 (2023). https://doi.org/10.1016/j.compstruct.2022.116370.

[20] A. Catapano, M. Montemurro, A multi-scale approach for the optimum design of sandwich plates with honeycomb core. Part I: Homogenisation of core properties, Compos. Struct. 118 (2014) 664–676. https://doi.org/10.1016/j.compstruct.2014.07.057.

[21] J. Yvonnet, Computational Homogenization of Heterogeneous Materials with Finite Elements, Springer International Publishing, Cham, 2019. https://doi.org/10.1007/978-3-030-18383-7.

[22] L.J. Gibson, M.F. Ashby, The mechanics of honeycombs, in: Cell. Solids, Cambridge University Press, 2014: pp. 93–174. https://doi.org/10.1017/cbo9781139878326.006.

[23] D. Nikiema, P. Balland, A. Sergent, Experimental and numerical investigations of 3D-printed Onyx parts reinforced with continuous glass fibers, Arch. Civ. Mech. Eng. 24 (2024) 50. https://doi.org/10.1007/s43452-024-00861-5.

[24] A. Avanzini, D. Battini, L. Giorleo, Finite element modelling of 3D printed continuous carbon fiber composites: Embedded elements technique and experimental validation, Compos. Struct. 292 (2022). https://doi.org/10.1016/j.compstruct.2022.115631.

[25] A. Tessarin, M. Zaccariotto, U. Galvanetto, D. Stocchi, A multiscale numerical homogenization-based method for the prediction of elastic properties of components produced with the fused deposition modelling process, Results Eng. 14 (2022). https://doi.org/10.1016/j.rineng.2022.100409.

[26] L. Viet Dung, N. Quang Hung, D. Pham Tuong Minh, C. Author, A numerical model for the honeycomb core sandwich panels in three-point bending by the homogenization method, n.d. www.ijres.org.